Clinical and Translational Radiation Oncology 45 (2024) 100737

Contents lists available at ScienceDirect

Clinical and Translational Radiation Oncology

journal homepage: www.sciencedirect.com/journal/clinical-and-translational-radiation-oncology

Early radiologic and metabolic tumour response assessment during combined chemo-radiotherapy for locally advanced NSCLC

Marie Tvilum [a,b,*], Marianne Marquard Knap [a], Lone Hoffmann [a,c], Azza Ahmed Khalil [a], Ane L. Appelt [d,e], Ate Haraldsen [f], Markus Alber [g,h], Cai Grau [b], Hjørdis Hjalting Schmidt [a], Maria Kandi [a], Marianne Ingerslev Holt [i], Christina Maria Lutz [a,1], Ditte Sloth Møller [a,c,1]

[a] Department of Oncology, Aarhus University Hospital, Denmark
[b] Danish Center for Particle Therapy, Aarhus University Hospital, Denmark
[c] Department of Clinical Medicine, Faculty of Health Sciences, Aarhus University, Denmark
[d] Leeds Institute of Medical Research at St James's, University of Leeds, United Kingdom
[e] Leeds Cancer Centre, Leeds Teaching Hospitals NHS Trust, Leeds, United Kingdom
[f] Department of Nuclear Medicine and PET-centre, Aarhus University Hospital, Denmark
[g] Department of Radiation Oncology, Heidelberg University Hospital, Germany
[h] Heidelberg Institute for Radiation Oncology (HIRO), Heidelberg University Hospital, Germany
[i] Department of Clinical Genetics, Sygehus Lillebaelt, Vejle, Denmark

ARTICLE INFO

Keywords:
Non-small cell lung cancer
Early treatment response
Pattern of failure

ABSTRACT

Background: The role of early treatment response for patients with locally advanced non-small cell lung cancer (LA-NSCLC) treated with concurrent chemo-radiotherapy (cCRT) is unclear. The study aims to investigate the predictive value of response to induction chemotherapy (iCX) and the correlation with pattern of failure (PoF).
Materials and methods: Patients with LA-NSCLC treated with cCRT were included for analyses (n = 276). Target delineations were registered from radiotherapy planning PET/CT to diagnostic PET/CT, in between which patients received iCX. Volume, sphericity, and SUVpeak were extracted from each scan. First site of failure was categorised as loco-regional (LR), distant (DM), or simultaneous LR+M (LR+M). Fine and Gray models for PoF were performed: a baseline model (including performance status (PS), stage, and histology), an image model for squamous cell carcinoma (SCC), and an image model for non-SCC. Parameters included PS, volume (VOL) of tumour, VOL of lymph nodes, ΔVOL, sphericity, SUVpeak, ΔSUVpeak, and oligometastatic disease.
Results: Median follow-up was 7.6 years. SCC had higher sub-distribution hazard ratio (sHR) for LRF (sHR = 2.771 [1.577:4.87], $p < 0.01$) and decreased sHR for DM (sHR = 0.247 [0.125:0.485], $p < 0.01$). For both image models, high diagnostic SUVpeak increased risk of LRF (sHR = 1.059 [1.05:1.106], $p < 0.01$ for SCC, sHR = 1.12 [1.03:1.21], $p < 0.01$ for non-SCC). Patients with SCC and less decrease in VOL had higher sHR for DM (sHR = 1.025[1.001:1.048] pr. % increase, p = 0.038).
Conclusion: Poor response in disease volume was correlated with higher sHR of DM for SCC, no other clear correlation of response and PoF was observed. Histology significantly correlated with PoF with SCC prone to LRF and non-SCC prone to DM as first site of failure. High SUVpeak at diagnosis increased the risk of LRF for both histologies.

Introduction

State-of-the-art treatment for patients with locally advanced non-small cell lung cancer (LA-NSCLC) consists of concurrent chemo-radiotherapy (cCRT), followed by adjuvant immunotherapy for selected patients [1,2]. Modern radiotherapy techniques allow treatment doses of 60–66 Gy in 30–33 fractions delivered with intensity-modulated radiotherapy (IMRT) and image-guidance [3]. Nevertheless, disease control rates and overall survival are poor, with two-year progression free survival of around 30 % without, and 45 % with

* Corresponding author at: Department of Oncology and Danish Centre for Particle Therapy, Palle Juul-Jensens Boulevard, 99 8200 Aarhus N, Denmark.
E-mail address: matvpe@rm.dk (M. Tvilum).
[1] These authors are shared last authorship.

https://doi.org/10.1016/j.ctro.2024.100737
Received 2 November 2023; Received in revised form 20 January 2024; Accepted 21 January 2024
Available online 23 January 2024

adjuvant immunotherapy [4,5]. One way to improve treatment outcome could be to increase the radiotherapeutic dose. Unfortunately, studies have shown that homogenous dose escalation to an unselected group of patients is toxic [6,7], and patient selection is thus essential for future attempts at local or systemic treatment intensification. Patient selection and eligibility are currently based on clinical baseline data such as stage and performance status (PS). However, several studies have suggested that early radiologic (CT-based) and metabolic (positron emission tomography (PET)-based) response to treatment might add predictive value, and a variety of metrics at different timepoints of the treatment course have been investigated [8–21]. Unfortunately, most studies are limited by small patient numbers, different timepoints of measuring response, incompatible endpoints, and conflicting results. Usmanij et al. [11] found that a reduction in total lesion glycolysis (TLG) during cCRT was associated with improved progression-free-survival (PFS), while Kong et al. [10] found that a reduction in mid-treatment FDG-PET volumes was associated with worse overall survival (OS). Kanzaki et al. [18] showed that early regression in tumour volume was significantly associated with improved PFS and OS for patients with squamous cell carcinomas (SCC) as opposed to patients with adenocarcinomas (AC). In contrast, Brink et al. [19] found that regression in tumour volume measured on cone-beam CT during RT was correlated with poorer OS for patients with non-adenocarcinoma histology. In some countries, one series of induction chemotherapy is administered for patients with LA-NSCLC while radiotherapy is planned. In such a setting, response after induction chemotherapy seems like a logical timepoint for response evaluation. McAleer et al. [22] found poorer OS for patients with stable or progressive disease after induction chemotherapy. However, this response was measured using X-ray images in a cohort of 141 evaluable patients. Larger cohorts evaluated with contemporary imaging tools are needed to explore the predictive value of treatment response, hereby adding supportive information for tailoring treatment decisions based on individualized risk stratification as early in the treatment course as possible.

The aim of the current study was to evaluate whether radiologic or metabolic tumour response after induction chemotherapy, and prior to start of radiotherapy, is correlated with pattern of failure for patients with LA-NSCLC treated with combined chemo-radiotherapy.

Materials and methods

Patients

Patients with LA-NSCLC treated consecutively with cCRT at a single institution from 2012 to 2018 were considered for the current analysis. Patients were included if they had received 1–2 series of platinum-based induction chemotherapy and a total homogenous radiation dose of 60 Gy-66 Gy in 30–33 fractions. This mainly included patients with stage III disease, but patients with stage I-II disease not eligible for surgery as well as patients with oligometastatic disease treated with local ablative therapy preceding the course of cCRT were allowed. The study investigated radiologic and metabolic changes between the diagnostic PET/CT scan (dPCT) and the radiotherapy planning PET/CT scan (pPCT), in between which patients received induction chemotherapy (Fig. 1). Patients were excluded in case of missing dPCT or pPCT (n = 27), if one of the scans were performed in deep inspiration breath hold (n = 11), or at lack of access to the attenuation corrected PET-scan (n = 4). Patients with <7 days from first chemotherapeutic infusion to pPCT (n = 14) as well as patients with >60 days between dPCT and first chemotherapeutic treatment (n = 6) were excluded. Patients who received intrathoracic surgical intervention or radiofrequency ablation as a part of their treatment regimen were also excluded (n = 17), while patients receiving explorative thoracotomy were permitted. One patient included diagnosed with two synchronous lung cancers had one tumour-site resected followed by concurrent chemo-radiotherapy at the other. In total, 276 patients were eligible for analysis. The study was approved by the Danish Data Protection Agency and the Danish National Board of Health (3-3013-2756/1).

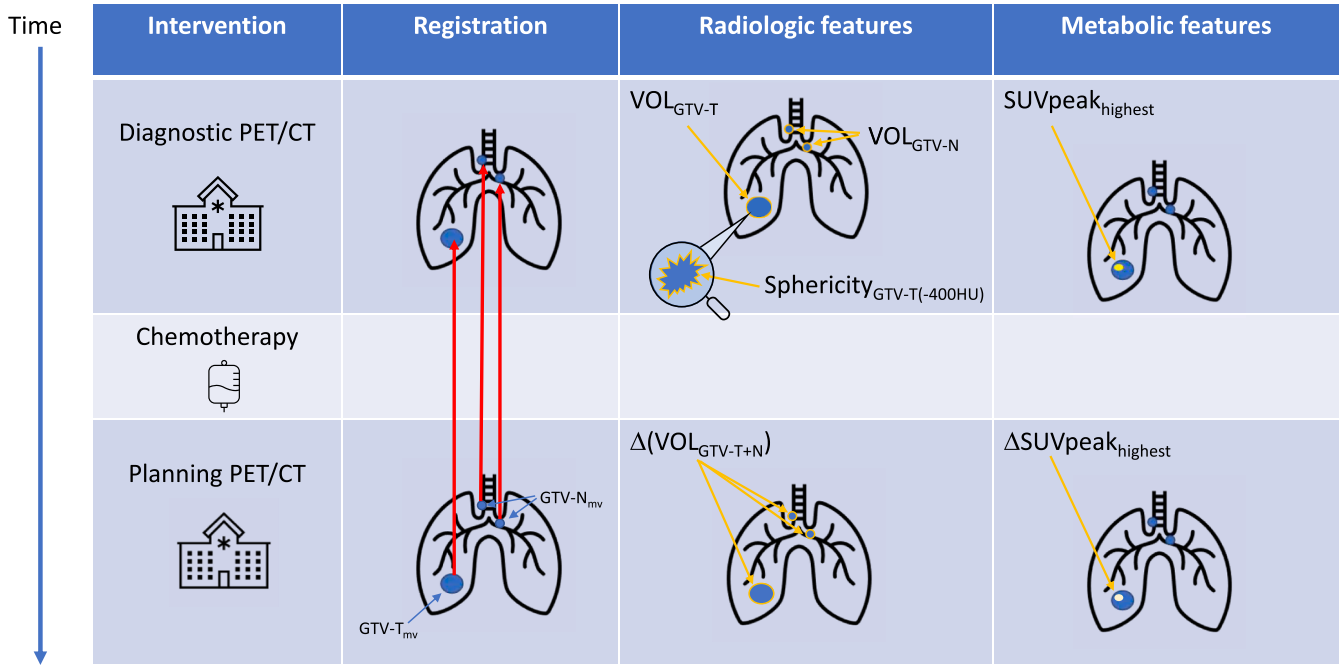

Fig. 1. Study design. Mid-ventilation planning target structures of GTV-T and GTV-N were registered from the planning PET/CT to the diagnostic PET/CT and corrected if needed. Features for response assessment were extracted from each scan. These included radiologic features (volume and sphericity) in addition to the metabolic feature of SUV_{peak}. The change in total disease volume (Δ ($VOL_{GTV\text{-}T+N}$)) was calculated from the diagnostic to the planning CT. The lesion with the highest SUV_{peak} on the diagnostic PET was identified on the planning PET and the change (Δ $SUVpeak_{highest}$) was calculated. Abbreviations, GTV-T: gross volume of target tumour, GTV-N: gross volume of target lymphnodes, GTV-T(−400HU): gross volume of target tumour subtracted Hounsfield units below 400 (air).

Staging and treatment

All patients were staged by [18F]-fluorodeoxyglucose positron emission tomography, magnetic resonance imaging of the brain, and the diagnosis confirmed by biopsy of tumour and/or lymph nodes. Diagnostic PET/CT scans were performed at regional hospitals before referral to treating institution. All dPCT were performed according to international guidelines, while scanners and reconstruction algorithms varied between different institutions. The pPCT was performed at the same scanner for almost all patients (n = 260). An overview of the scanners and reconstruction algorithms is presented in Supplementary Table 1.

Patients were treated with either cisplatin or carboplatin in combination with oral vinorelbine day 1 and 8 in each cycle. Treatment planning was performed in Eclipse (Varian Medical Systems). Gross tumour volume (GTV-T) and lymph nodes (GTV-N) were defined on the pPCT by an experienced radiation oncologist in collaboration with an experienced radiologist and an experienced nuclear medicine specialist. Radiotherapy treatment was delivered as standard homogenous doses of 2 Gy/fraction/5 fractions weekly with daily treatment setup imaging (Cone-beam CT). Match on thoracic vertebrae (n = 51) or match on tumour (n = 225) with adaptive radiotherapy was used for setup [23,24]. For the cohort considered, immunotherapy was not yet standard-of-care in the adjuvant setting. Thus, no patients received this as a part of their curative treatment strategy.

Response assessment and data collection

Diagnostic PET/CT (baseline) and pPCT were collected for each patient and co-registered deformably using MIM 7.2.1™ (MIM Software, Cleveland, OH). Mid-ventilation planning target structures of GTV-T and GTV-N were deformably transferred from the pPCT to the dPCT, and manually adjusted if needed (Fig. 1) to ensure that they covered all visible tumour tissue on the dPCT. Features for response assessment were preselected based on literature search and extracted from each scan. These included radiologic measurements (volume and surface area) of GTV-T and GTV-N, in addition to peak standardized uptake value (SUV_{peak}) on PET. SUV_{peak} was chosen since it has been shown to be a robust response predictor across observers and reconstruction algorithms [25–27]. GTV-N was subdivided into each lymph node-lesion, and each lesion was identified on each scan to extract comparative parameters.

After the end of treatment, patients had follow-up visits and CT-scans scheduled every third month for the first two years and subsequently every six months for additional three years. First site of failure was defined as either loco-regional (LRF), distant (DM) or simultaneous LRF + DM by reviewing imaging, the radiologic description, and patient records. Loco-regional failure was defined as failure in the irradiated region and/or regional lymph nodes, whereas distant failure was defined as spread to distant organs according to TNM Classification system [28].

Analysis

Index date was the date of pPCT. Date of first failure was defined as the date of the first scan where the failure was detected and subsequently confirmed by biopsy. Patients were censored after first failure. P-values < 0.05 were considered statistically significant. As all variables presented in Table 2 were continuous, Mann-Whitney U tests were performed for comparison. Median follow-up was calculated by reverse Kaplan-Meier estimate.

Multivariate competing risk analysis was performed using Fine and Gray (F&G) as the primary method. Additional Cox proportional hazard analyses were performed and reported in Supplementary material for comparison and evaluation of the robustness of the findings to the model assumptions. Three models were generated for both F&G and Cox: a baseline clinical model and two image models. The baseline clinical model included all patients in the cohort and included predefined baseline characteristics: PS, stage (grouped in ≤IIB, IIIA and ≥IIIB) and histology. Two separate image models were evaluated for SCC and non-SCC patients, as previous studies have reported different patterns of failure depending on histology [29,30]. The image-models comprised the following parameters: PS, volume (VOL) of GTV-T on dPCT, VOL of GTV-N on dPCT, difference in total disease volume (Δ ($VOL_{GTV-T+N}$)), sphericity of GTV-T on dPCT, SUV_{peak} on dPCT and difference in SUV_{peak} (Δ SUV_{peak}). Metastasis at diagnosis was only considered a parameter in the image model for non-SCC histology, as 20 of 21 patients with oligometastatic disease had non-SCC. Stage is strongly correlated with volume of GTV-T, GTV-N and metastasis at diagnosis and thus not included in the image models as a separate parameter.

If more than one T-site was present, the volume of GTV-T was calculated as the sum of all T-sites. The total disease volume ($VOL_{GTV-T+N}$) was the sum of all tumour and lymph node lesions. For SUV_{peak}, the target with the highest SUV_{peak} on the dPCT was chosen and tracked to the pPCT. SUV_{peak} for the same target on the pPCT was extracted, and the differences between the values on dPCT and pPCT was calculated. For the majority of patients, the target lesion with the highest SUV_{peak} was T-site (n = 200). Delta parameters for both GTV and SUV_{peak} were defined as:

Table 1
Patient- and treatment characteristics for full cohort and stratified by histology.

Patient characteristics	Full cohort n = 276	Non-SCC n = 177	SCC n = 99
Gender, n (%)			
Male	144 (52.2)	70 (39.5)	74 (74.7)
Female	132 (47.8)	107 (60.5)	25 (25.3)
Performance-status, n (%)			
0	108 (39.1)	72 (40.7)	36 (36.4)
1	139 (50.4)	89 (50.3)	50 (50.5)
2	29 (10.5)	16 (9.0)	13 (13.1)
Stage, n (%)			
I	10 (3.6)	4 (2.3)	6 (6.1)
II	25 (9.1)	9 (5.1)	16 (16.1)
IIIA	124 (44.9)	80 (45.2)	44 (44.4)
IIIB	79 (28.6)	53 (29.9)	26 (26.3)
IIIC	17 (6.2)	11 (6.2)	6 (6.1)
IV	21 (7.6)	20 (11.3)	1 (1.0)
Age (years)			
Median (IQR)	67 (60–73)	66 (59–71)	69 (63–75)
Treatment characteristics			
Chemotherapy agent, n (%)			
Cisplatin	109 (39.5)	72 (40.7)	37 (37.4)
Carboplatin	166 (60.1)	104 (58.8)	62 (62.6)
Vinorelbine only	1 (0.4)	1 (0.6)	0
Dose (Gy), n (%)			
60	41 (14.9)	29 (16.4)	12 (12.1)
64	2 (0.7)	2 (1.1)	0
66	233 (84.4)	146 (82.5)	87 (87.9)
Days from diagnostic PET/CT to chemotherapy, *Median, IQR*	26 (20–33)	27 (21–34)	25 (19–30)
Days from chemotherapy to planning PET/CT *Median, IQR*	13 (10–25)	13 (10–23)	13 (10–28)

Abbreviations: SCC: squamous cell carcinoma, IQR: inter quartile range, Gy: Gray.

Table 2
Image features stratified by histology.

Feature	No site to evaluate (n)	Non-SCC (n = 177)	SCC (n = 99)	P-value[a]
Diagnostic GTV-T Volume (mL), median (IQR)	35	42.64 (13.04–95.58)	56.01 (20.53–124.56)	0.094
Diagnostic GTV-N Volume (mL), median (IQR)	53	11.84 (5.02–25.17)	10.87 (5.24–17.11)	0.268
Δ Disease volume in %, median (IQR)	0	−16.13 (−25.04:−8.24)	−16.2 (−25.81:−8.8)	0.998
Diagnostic Sphericity of GTV-T_{-400HU}, median (IQR)	35	0.7926 (0.7096–0.8682)	0.747 (0.6429–0.8459)	0.063
Diagnostic Highest SUV_{peak}, median (IQR)	0	11.07 (7.54–14.51)	13.18 (9.55–17.05)	< 0.01
Δ Highest SUV_{peak} in %, median (IQR)	0	−34.86 (−49.64:−21.8)	−36.13 (−48.2:−23.42))	0.912

Abbreviations: SCC: squamous cell carcinomas, GTV-T: gross tumour volume, IQR: interquartile range, GTV-N: gross lymphnode volume, GTV-T_{-400HU}: gross tumour volume subtracted Hounsfield units below −400 (air), SUV: standardized uptake value.
[a] Mann-Whitney U Test.

$$\Delta parameter(\%) = \frac{Value_{PlanningScan} - Value_{DiagnosticScan}}{Value_{DiagnosticScan}} \times 100$$

If baseline (extracted from dPCT) volume was ≤4 mL (n = 2) or baseline SUV_{peak} was ≤4 (n = 10), the difference in total disease volume or SUV_{peak} was fixed to 0 due to unreliability of estimates for small volumes and SUV_{peak} at background level.

Finally, sphericity has previously been shown to be strongly associated with survival in a univariate model [31], and was hence included as a feature in this study. To calculated sphericity, surrounding air (defined as Hounsfield units with values below −400) was subtracted from the GTV-delineation of the largest tumour (GTV-T_{-400HU}) to get a true measure of sphericity, see Supplementary Fig. 1. For this tight-fitted tumour delineation, sphericity was calculated according to the Image Biomarker Standardization Initiative [32]:

$$Sphericity = \frac{\left(36\pi \times Volume^2\right)^{1/3}}{Surfacearea}$$

Thus, a sphericity of 1 represents the shape of a sphere. Patients without primary tumour (n = 35) were assigned the median sphericity of the remaining patients (i.e. univariate imputation by median value).

Subdistribution hazard ratios (sHR) were reported for all models. For subgroups, pattern of failure was visualised with stacked incidence plots of first site of failure. All statistical analyses were performed using IBM SPSS Statistics 28.0 and R version 4.2.2.

Results

The full cohort included 177 patients with non-SCC and 99 patients with SCC. Median follow-up was 7.6 years (95 %CI: [6.9–8.8]). Median OS for the full cohort was 28.3 months (95 %CI: [24.1–35.6]). Baseline patient- and treatment characteristics for the full cohort and split on histology are presented in Table 1. In general, slightly more patients were male, the majority had a performance status of 0–1 and presented with locally advanced disease. Most patients received a radiation dose of 66 Gy/33 fractions (n = 233) in combination with carboplatin. Extracted radiologic and metabolic image features stratified by histology are presented in Table 2. Diagnostic SUV_{peak} was significantly higher for patients with SCC. In terms of both change in volume and SUV_{peak}, most patients experienced a decrease. No differences in the response after induction of chemotherapy were observed across histologies.

The baseline clinical model for the full cohort (Table 3) shows a clear association between sub-distributed histology and pattern of failure. Patients with SCC seem more prone to loco-regional failure (sHR: 2.771, 95 % confidence interval (CI) [1.577:4.87], p < 0.01) and less prone to distant failure (sHR: 0.247, 95 % CI [0.125:0.485], p < 0.01) compared to patients with non-SCC. Meanwhile, the results also indicate that more patients with SCC in our cohort die with no evidence of disease (DNED) (sHR: 2.572, [1.332:4.969], p < 0.01) compared to non-SCC. Patients with PS 0 seem less likely to experience DNED as first event compared to patients with PS 1 or 2 (sHR: 0.419, 95 %CI [0.192:0.915], p = 0.029) but are more prone to LRF + DM failure as first event (sHR: 1.63, 95 %CI [1.002:2.65], p = 0.049).

The image model for non-SCC (Table 4, left) shows increased risk of LRF for PS 0 (sHR: 2.7, 95 % CI [1.15:6.32], p = 0.022), large GTV-T volume (sHR: 1.03 pr 10 mL increase, 95 %CI: [1.02:1.05], p < 0.01) and high SUV_{peak} at baseline (sHR: 1.12, 95 %CI [1.03:1.21], p < 0.01), compared to the risk of failing distant, simultaneously, or die without recurrence. Stage IV-disease at baseline was significantly associated with increased risk of failing distantly as first event (sHR: 3.798, 95 % CI

Table 3
Fine & Gray competing risk baseline clinical model for pattern of first failure.

Failure	Parameter	Unit	Full cohort (n = 276) sHR [95 % CI], *p*-value
LRF n = 54	*PS*	0 vs. 1 or 2	0.864 [0.49:1.52], p = 0.61
	Stage	Stage ≤ IIB vs. IIIA	1.072 [0.492:2.34], p = 0.86
		Stage ≥ IIIB vs IIIA	1.002 [0.54:1.86], p = 0.99
	Histology	SCC vs. non-SCC	**2.771 [1.577:4.87], p < 0.01**
DM n = 79	*PS*	0 vs. 1 or 2	1.122 [0.718:1.754], p = 0.61
	Stage	Stage ≤ IIB vs. IIIA	1.31 [0.549:3.128], p = 0.54
		Stage ≥ IIIB vs. IIIA	**1.64 [1.034:2.599], p = 0.035**
	Histology	SCC vs. non-SCC	**0.247 [0.125:0.485], p < 0.01**
LRF + DM n = 66	*PS*	0 vs. 1 or 2	**1.63 [1.002:2.65], p = 0.049**
	Stage	Stage ≤ IIB vs. IIIA	1.13 [0.526:2.43], p = 0.75
		Stage ≥ IIIB vs. IIIA	1.36 [0.803:2.30], p = 0.25
	Histology	SCC vs. non-SCC	0.92 [0.545:1.55], p = 0.75
DNED n = 37	*PS*	0 vs. 1 or 2	**0.419 [0.192:0.915], p = 0.029**
	Stage	Stage ≤ IIB vs. IIIA	1.215 [0.525:2.814], p = 0.65
		Stage ≥ IIIB vs. IIIA	0.848 [0.398:1.806], p = 0.67
	Histology	SCC vs. non-SCC	**2.572 [1.332:4.969], p < 0.01**

Abbreviations: sHR: subdistributed hazard rate, CI: confidence interval, LRF: Loco-regional failure, DM: Distant metastases, DNED: Death no evidence of disease, PS: Performance status, SCC: squamous cell carcinoma.

Table 4
Fine & Gray competing risk model for pattern of failure split by histology.

Site of failure	Parameter	Unit	Non-Squamous Cell Carcinomas (n = 177) sHR [95 % CI], *p*-value	Squamous Cell Carcinomas (n = 99) sHR [95 % CI] *p*-value
LRF	*PS*	0 vs. 1 or 2	**2.7 [1.15:6.32], p = 0.022***	0.464 [0.187:1.153], p = 0.098
	GTV-T$_{Diagnosis}$	pr 10 mL	**1.03 [1.02:1.05], p < 0.01***	0.99 [0.949:1.032], p = 0.64
	GTV-N$_{Diagnosis}$	mL	0.989 [0.957:1.02], p = 0.51	**0.949 [0.905:0.994], p = 0.027***
	Δ Total disease volume	%	1.02 [1.00:1.04], p = 0.059	1.009 [0.978:1.038], p = 0.62
	Highest SUV$_{peak,\ Diagnosis}$	mBq	**1.12 [1.03:1.21], p < 0.01***	**1.059 [1.05:1.106], p < 0.01***
	Sphericity GTV-T$_{.400\ HU,\ Dia}$		1.00 [0.978:1.03], p = 0.77	0.985 [0.952:1.019], p = 0.38
	Δ SUV$_{peak,\ tracked\ structure}$	%	1.00 [0.989:1.01], p = 0.96	0.998 [0.981:1.016], p = 0.86
	Oligometastasis$_{Diagnosis}$	Yes vs. no	**1.21×10^{-6} [5.72×10^{-7}:2.56×10^{-6}], p < 0.01**	–
DM	*PS*	0 vs. 1 or 2	1.196 [0.716:2.00], p = 0.49	0.779 [0.199:3.055], p = 0.72
	GTV-T$_{Diagnosis}$	pr 10 mL	1.00 [0.982:1.02], p = 0.98	**0.885 [0.802:0.976], p = 0.015**
	GTV-N$_{Diagnosis}$	mL	**1.012 [1.002:1.02], p = 0.024***	0.989 [0.954:1.025], p = 0.55
	Δ Total disease volume	%	1.007 [0.992:1.02], p = 0.36	**1.025 [1.001:1.048], p = 0.038***
	Highest SUV$_{peak,\ Diagnosis}$	mBq	0.966 [0.919:1.01], p = 0.17	1.064 [0.977:1.157], p = 0.15
	Sphericity GTV-T$_{.400\ HU,\ Diagnosis}$	pr. 0.01	0.99 [0.97:1.01], p = 0.37	1.008 [0.959:1.06], p = 0.75
	Δ SUV$_{peak,\ tracked\ structure}$	%	1.003 [0.995:1.01], p = 0.44	1.011 [0.976:1.047], p = 0.55
	Oligometastasis$_{Diagnosis}$	Yes/ no	**3.798 [1.921:7.51], p < 0.01***	–
LRF + DM	*PS*	0 vs. 1 or 2	1.129 [0.612:2.08], p = 0.7	**3.284 [1.325:8.137], p = 0.01**
	Vol GTV-T$_{Diagnosis}$	pr 10 mL	0.988 [0.959:1.02], p = 0.44	1.022 [0.985:1.06], p = 0.25
	Vol GTV-N$_{Diagnosis}$	mL	1.004 [0.994:1.01], p = 0.47	**1.029 [1.008:1.049], p < 0.01**
	Δ Total disease volume	%	0.996 [0.973:1.02], p = 0.72	1.019 [0.992:1.047], p = 0.17
	Highest SUV$_{peak,\ Diagnosis}$	mBq	0.953 [0.89:1.02], p = 0.17	1.000 [0.936:1.068], p = 1.0
	Sphericity GTV-T$_{.400\ HU,\ Diagnosis}$	pr 0.01	0.992 [0.968:1.02], p = 0.52	**0.957 [0.927:0.988], p < 0.01***
	Δ SUV$_{peak,\ tracked\ structure}$	%	0.994 [0.98:1.01], p = 0.35	1.017 [0.992:1.042], p = 0.19
	Oligometastasis$_{Diagnosis}$	Yes/ no	0.763 [0.24:2.42], p = 0.65	–
DNED	*PS*	0 vs. 1 or 2	0.201 [0.04:1.02], p = 0.052	0.582 [0.205:1.65], p = 0.31
	GTV-T$_{Diagnosis}$	pr 10 mL	0.923 [0.815:1.05], p = 0.21	**1.054 [1.012:1.1], p = 0.011***
	GTV-N$_{Diagnosis}$	mL	0.986 [0.952:1.02], p = 0.43	1.012 [0.998:1.03], p = 0.091
	Δ Total disease volume	%	1.014 [0.963:1.07], p = 0.6	0.965 [0.93:1.0], p = 0.056
	Highest SUV$_{peak,\ Diagnosis}$	mBq	1.068 [0.99:1.15], p = 0.089	**0.882 [0.81:0.96], p < 0.01**
	Sphericity GTV-T$_{.400\ HU,\ Diagnosis}$	pr. 0.01	1.026 [0.969:1.09], p = 0.38	**1.036 [1.003:1.07], p = 0.034**
	Δ SUV$_{peak,\ tracked\ structure}$	%	1.008 [0.984:1.03], p = 0.53	1.002 [0.986:1.02], p = 0.79
	Oligometastasis$_{Diagnosis}$	Yes/ no	0.504 [0.084:3.03], p = 0.45	–

Values marked with * are values and parameters also indicating significant correlation in the Cox proportional hazards model presented in the Supplementary Table 3. Abbreviations: sHR: subdistributed hazard ratio, CI: confidence interval, LRF: Loco-regional failure, DM: Distant metastases, LRF + DM: Simoultaneous loco-regional and distant failure, DNED: death no evidence of disease, PS: performance status, GTV-T: gross tumour volume, GTV-N: gross lymphnode volume, SUV: standardized uptake value, HU: Houndsfield Units, mBq: megaBecquerel.

[1.921:7.51], p < 0.01). Further, increased risk of DM was observed for large GTV-N (sHR: 1.012 pr. mL increase, 95 %CI [1.002:1.02], p = 0.024). No associations were found between any parameters and LRF + DM or DNED.

The image model for SCC (Table 4, right) shows increased risk of LRF for high SUV_{peak} at baseline (sHR: 1.059, 95 %CI [1.05:1.106], p < 0.01), while an increased risk of DM was observed for patients with minor response in total disease volume (sHR: 1.025 pr. % increase, 95 % CI [1.001:1.048], p = 0.038). Patients with large GTV-N volumes (sHR: 1.029 pr. mL increase, 95 %CI [1.008:1.049], p < 0.01) and PS 0 (sHR: 3.284, 95 %CI: [1.325:8.137], p = 0.01) presented a higher risk of simultaneous LRF and DM. For patients with large GTV-T volume at baseline (sHR: 1.054 pr. 10 mL increase, 95 %CI [1.012:1.1], p = 0.011] and high sphericity (sHR: 1.036, 95 %CI: [1.003:1.07], p = 0.034) the risk of DNED was higher.

Similar hazards for both histologies are observed in the Cox proportional hazards model presented in Supplementary Table 3, although not all parameters showed clear significance in both models. Cumulative incidence plots for pattern of failure divided by the respective median SUV_{peak} for non-SCC and SCC are shown in Fig. 2. Besides indicating that pattern of failure is histology-dependent, the plots also demonstrate the correlation between baseline SUV_{peak} and the risk of loco-regional failure, especially for patients with non-SCC. In addition, Fig. 2 also indicates that some patients experienced death with no evidence of disease less than a year after their pPCT.

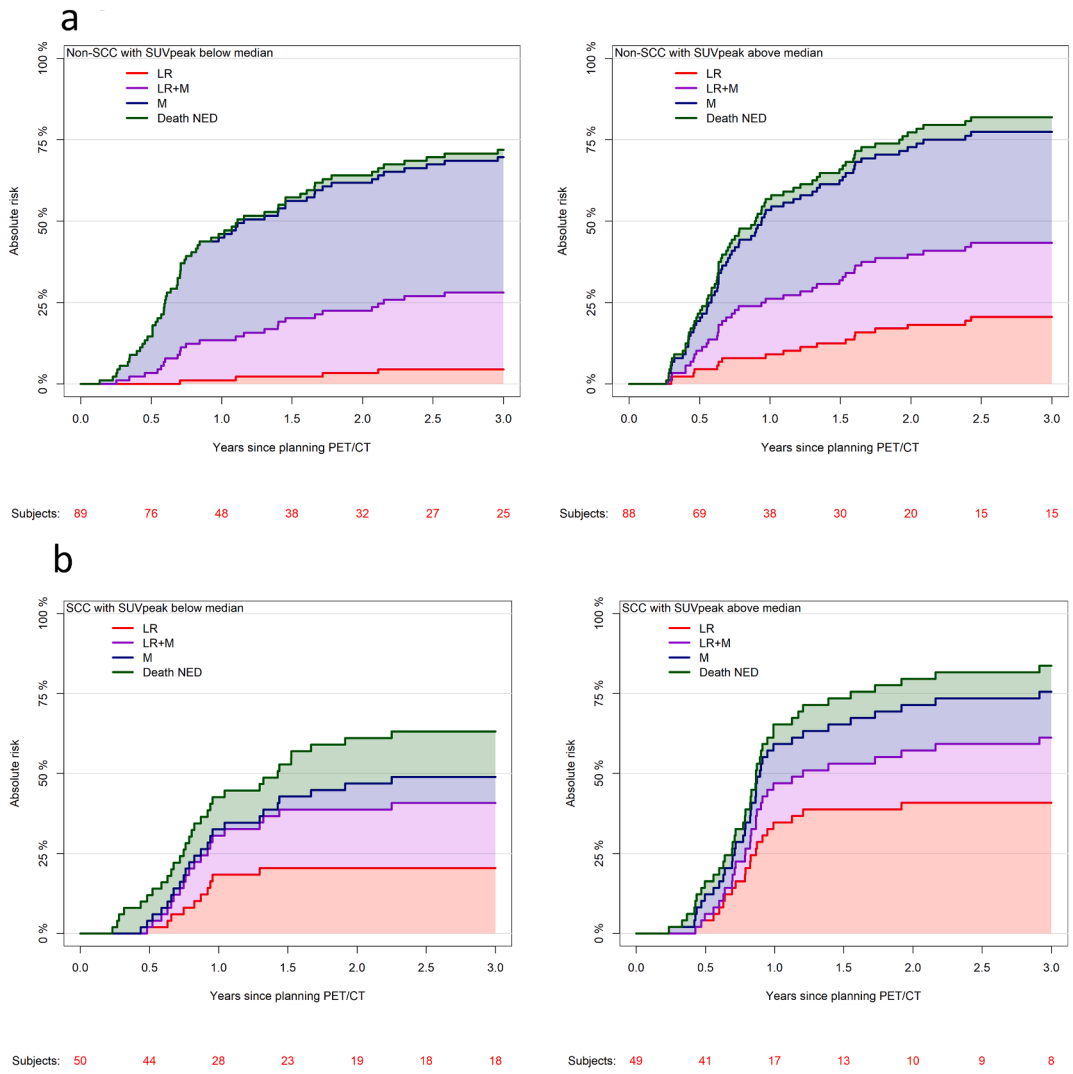

Fig. 2. Cumulative incidence plots of pattern of failure for patients with non-SCC (a) and SCC (b) divided by SUV_{peak} below (left) and above (wright), the respective median SUV_{peak}.

Discussion

This study evaluated if diagnostic PET/CT imaging or response to induction chemotherapy were predictive of pattern of failure for patients with LA-NSCLC treated with curatively intended cCRT. The findings of the study suggest that less decrease in total disease volume after induction chemotherapy is significantly associated with an enhanced risk of distant failure for patients with SCC. Additionally, the results of this study clearly state a correlation between histology and risk of LRF and DM failure, while SUV_{peak} at baseline was significantly associated with risk of loco-regional failure across histology.

In the baseline clinical model presented in Table 3, SCC were significantly more prone to LR failure than DM compared to patients with non-SCC histology. This is in accordance with previous studies [29,30,33]. The result indicates that histology is an important prognostic factor for pattern of failure. Further, patients with PS 0 seem less likely to die with no evidence of disease than patients with performance status 1 or 2, but more likely to experience recurrence. Be aware, that it lies in the interdependent nature of the competing risk analysis that subdistribution hazards and sHR for specific outcomes cannot be interpreted in isolation but are influenced by the competing risks. Thus, low PS does not increase the risk of recurrence, but patients with good PS are less likely to experience DNED as first event and are consequently more likely to present a recurrence while under follow-up for the study. All other results should be interpreted with similar caution.

In the image models presented in Table 4, increased GTV-T and GTV-N volumes enhanced the sHR of LRF and DM, respectively, for patients with non-SCC. Additionally, metastases at diagnoses significantly increased the risk of DM as first failure (Table 4, left). Similar correlation between baseline radiologic features were found for patients with SCC (Table 4, right). These findings might be a reflection of the strong correlation of the three parameters and stage, which is previously confirmed to be one of the most important prognostic factors in itself [34]. Although stage is a reasonable representation of a highly complex construct in many cases, it seemed too simple an approximation in this context of predictive modelling, where more detailed data were available.

Sphericity was included in the model to investigate whether tumour shape would add any predictive value. Our data suggest a trend towards more sphere-like tumours for patients with non-SCC (Table 2, $p = 0.063$). The image model for SCC shows that increasing sphericity (the more sphere-like the tumour is) decreases the sHR of LRF + DM, whereas the risk of DNED increases with increased sphericity. The latter is not supported by the Cox model presented in Supplementary Table 3. Davey et al. [31] found sphericity to be associated with overall survival in a univariate model and correlated with tumour volume, mean lung dose, N- and T-stage. Even though sphericity in this study is based on the $GTV\text{-}T_{-400}$ and not the delineated GTV-T like the study from Davey et al.,

it could potentially be a surrogate for these underlying factors in this study as well.

The difference in total disease volume was the only response parameter that showed clear correlation with increased risk of DM for patients with SCC, while no correlation on the significance of early metabolic evaluation was observed. While many studies investigate the correlation between early response to treatment and overall survival [10,11,18–21], this is not the case for the relationship between early radiological and metabolic response to treatment and correlation to pattern of failure. Nygård et al. [13] found that lesion-specific time to progression was longer in lesions with major response in SUV_{peak}, and that SUV_{peak} at baseline could predict risk of specific lesion failure [29]. Our findings support a predictive value of baseline SUV_{peak}. Nevertheless, the best time point for response assessment is an area often discussed by experts, and studies investigating the optimal timepoint for response assessment during cCRT for patients with LA-NSCLC have found that both different timepoints and the longitudinal response-measurements had high prognostic value [14,15].

In the current study, a model was performed separately for each histology to enhance the prognostic potential of ^{18}FDG-PET-scans by interpreting SUV according to histology, as previously suggested by Schuurbiers et al. [35]. In support to these findings, Kim et al. [33] have previously reported that SUV_{max}, SUV_{mean}, TLG and MTV are generally higher for patients with SCC. However, while SUV_{max} and SUV_{mean} was significantly associated with loco-regional progression-free-survival for patients with AC, they found no significant relation for patients with SCC. Our results suggest that high SUV_{peak} at dPCT increases the hazard rate for LRF for both histologies, although the effect seems to be higher for patients with non-SCC (sHR 1.12, 95 % CI [1.03:1.21], p = 0.024) than patients with SCC (sHR 1.059, 95 %CI [1.05:1.106]). This could possibly reflect both differences in baseline SUV_{peak}, which is higher for SCC (Table 2), and SCC having a generally higher risk of LRF (Table 3). However, it seems as though a subgroup of non-SCC patients with high baseline SUV_{peak} have a high risk of LRF, very similar to SCC (see Fig. 2).

To reduce uncertainty of different treatment modalities interfering with pattern of failure, a full curatively intended course of RT (60–66 Gy) in addition to chemotherapy was required for inclusion in this study. This introduces a potential bias in the study, in addition to its mono-centric nature and the heterogeneity of stages included. Modern oncological treatment is pushing the border between locally advanced, and oligometastastic disease as more aggressive localized treatment options become available. We therefore chose to include patients who received curatively intended localized treatment for their oligometastatic disease in the model to have the patient population as representative of reality as possible, even though previous publications [36] indicate that the risk of distant failure is significantly higher for patients diagnosed with oligometastatic disease. Our findings support these results, and the conclusion of Mentink et al. [37], stating that patient selection for aggressive localized therapy in a curative setting seem crucial, as oligometastatic disease is a broad-spectrum disease with variable prognosis.

Regarding metabolic response assessment, the different reconstruction algorithms for dPCT and pPCT scans may potentially influence our results. To account for this, we used SUV_{peak} as the only metabolic parameter for response assessment, since this parameter was previously shown to be a robust response predictor across observers and reconstruction algorithms [25–27]. Furthermore, the response parameter of SUV_{peak} was fixed to a value of 0 if SUV_{peak} at baseline was less than 4, to account for unreliability of estimates for SUV_{peak}-values at background level.

The retrospective nature of the study resulted in a cohort not benefiting from current standard of care which nowadays includes adjuvant immunotherapy [38]. Nevertheless, we believe that results from this study remain relevant as the findings on the predictive value of imaging and histology are both hypothesis-generating and important for stratification when conducting future trials exploring pattern of failure for patients with LA-NSCLC.

In conclusion, the findings of this study demonstrate a clear correlation between pattern of failure and subdistributed histology, as patients with SCC were significantly more prone to LRF, while patients with non-SCC histology were more prone to DM. However, SUV_{peak} at baseline adds important prognostic value demonstrating a significantly increased risk of LRF with increasing SUV_{peak} for both histologies. Less decrease in total disease volume after chemotherapy was significantly associated with increased sHR of DM for patients with SCC, while no association between pattern of failure and metabolic response was observed for neither histology.

Funding statement

Marie Tvilum was supported by the Health Research Foundation of Central Denmark Region. Ditte Sloth Møller, Lone Hofmann and Marie Tvilum was supported by DCCC Radiotherapy – The Danish National Research Center for Radiotherapy, Danish Cancer Society (grant no. R191-A11526) and Danish Comprehensive Cancer Center. Ditte Sloth Møller, Christina Maria Lutz, Marianne Knap and Marie Tvilum was supported by Danish Cancer Society (grant no. R209-A13036 and R325-A18822). Christina Maria Lutz was supported by Danish Cancer Society (grant no. R90-A6244).

CRediT authorship contribution statement

Marie Tvilum: Methodology, Software, Validation, Formal analysis, Investigation, Resources, Writing – original draft, Visualization, Project administration. **Marianne Marquard Knap:** Investigation, Methodology, Resources, Writing – review & editing, Supervision. **Lone Hoffmann:** Methodology, Investigation, Writing – review & editing, Supervision. **Azza Ahmed Khalil:** Methodology, Investigation, Resources, Writing – review & editing, Supervision. **Ane L. Appelt:** Methodology, Formal analysis, Investigation, Writing – review & editing, Supervision. **Ate Haraldsen:** Methodology, Investigation, Writing – review & editing, Supervision. **Markus Alber:** Methodology, Writing – review & editing, Supervision. **Cai Grau:** Methodology, Writing – review & editing, Supervision. **Hjørdis Hjalting Schmidt:** Investigation, Resources, Writing – review & editing, Supervision. **Maria Kandi:** Investigation, Resources, Writing – review & editing, Supervision. **Marianne Ingerslev Holt:** Investigation, Resources, Writing – review & editing, Supervision. **Christina Maria Lutz:** Methodology, Investigation, Formal analysis, Writing – review & editing, Supervision, Data curation, Visualization. **Ditte Sloth Møller:** Methodology, Software, Supervision, Formal analysis, Data curation, Project administration, Visualization, Funding acquisition, Writing – review & editing.

Declaration of competing interest

The authors declare that they have no known competing financial interests or personal relationships that could have appeared to influence the work reported in this paper.

Appendix A. Supplementary data

Supplementary data to this article can be found online at https://doi.org/10.1016/j.ctro.2024.100737.

References

[1] Eberhardt WEE, De Ruysscher D, Weder W, et al. 2nd ESMO Consensus Conference in Lung Cancer: locally advanced stage III non-small-cell lung cancer. Ann Oncol 2015;26:1573–88. https://doi.org/10.1093/annonc/mdv187.

[2] Antonia SJ, Villegas A, Daniel D, et al. Durvalumab after chemoradiotherapy in stage III non-small-cell lung cancer. N Engl J Med 2017;377:1919–29. https://doi.org/10.1056/NEJMOA1709937.

[3] Nestle U, De Ruysscher D, Ricardi U, et al. ESTRO ACROP guidelines for target volume definition in the treatment of locally advanced non-small cell lung cancer. Radiother Oncol 2018;127:1–5. https://doi.org/10.1016/j.radonc.2018.02.023.
[4] Spigel DR, Faivre-Finn C, Gray JE, et al. Five-year survival outcomes from the PACIFIC trial: durvalumab after chemoradiotherapy in stage III non–small-cell lung cancer. JCO 2022;40:1301–11. https://doi.org/10.1200/JCO.21.01308.
[5] Møller DS, Lutz CM, Khalil AA, et al. Survival benefits for non-small cell lung cancer patients treated with adaptive radiotherapy. Radiother Oncol 2022;168:234–40. https://doi.org/10.1016/j.radonc.2022.01.039.
[6] Bradley JD, Paulus R, Komaki R, et al. Standard-dose versus high-dose conformal radiotherapy with concurrent and consolidation carboplatin plus paclitaxel with or without cetuximab for patients with stage IIIA or IIIB non-small-cell lung cancer (RTOG 0617): a randomised, two-by-two factorial p. Lancet Oncol 2015;16:187–99. https://doi.org/10.1016/S1470-2045(14)71207-0.
[7] Cooke SA, Dirk de Ruysscher P, Reymen B, et al. 18F-FDG-PET guided vs whole tumour radiotherapy dose escalation in patients with locally advanced non-small cell lung cancer (PET-Boost): results from a randomised clinical trial. Radiother Oncol 2023;109492. https://doi.org/10.1016/j.radonc.2023.109492.
[8] van Elmpt W, Öllers M, Dingemans A-M-C, et al. Response assessment using 18 F-FDG PET early in the course of radiotherapy correlates with survival in advanced-stage non-small cell lung cancer. J Nucl Med 2012;53:1514–20. https://doi.org/10.2967/jnumed.111.102566.
[9] Bowen SR, Hippe DS, Thomas HM, et al. Prognostic value of early fluorodeoxyglucose-positron emission tomography response imaging and peripheral immunologic biomarkers: substudy of a phase II trial of risk-adaptive chemoradiation for unresectable non-small cell lung cancer. Adv Rad Oncol 2022;7:100857. https://doi.org/10.1016/j.adro.2021.100857.
[10] Kong (Spring) F-M, Li L, Wang W, et al. Greater reduction in mid-treatment FDG-PET volume may be associated with worse survival in non-small cell lung cancer. Radiother Oncol 2019;132:241–9. https://doi.org/10.1016/j.radonc.2018.10.006.
[11] Usmanij EA, De Geus-Oei LF, Troost EGC, et al. 18F-FDG PET early response evaluation of locally advanced non-small cell lung cancer treated with concomitant chemoradiotherapy. J Nucl Med 2013;54:1528–34. https://doi.org/10.2967/JNUMED.112.116921.
[12] Fledelius J, Khalil AA, Hjorthaug K, Frøkiaer J. Using positron emission tomography (PET) response criteria in solid tumours (PERCIST) 1.0 for evaluation of 2′-deoxy-2′-[18F] fluoro-D-glucose-PET/CT scans to predict survival early during treatment of locally advanced non-small cell lung cancer (NSCLC): PERCIST 1.0 predicts response in NSCLC. J Med Imaging Radiat Oncol 2016;60:231–8. https://doi.org/10.1111/1754-9485.12427.
[13] Nygård L, Vogelius IR, Fischer BM, et al. Early lesion-specific (18)F-FDG PET response to chemotherapy predicts time to lesion progression in locally advanced non-small cell lung cancer. Radiother Oncol 2016;118:460–4. https://doi.org/10.1016/J.RADONC.2016.01.009.
[14] La Fontaine MD, Bruin NM, Van Kranen S, et al. The dynamics and prognostic value of FDG PET-metrics in weekly monitoring of (chemo)radiotherapy for NSCLC. Radiother Oncol 2021;160:107–14. https://doi.org/10.1016/j.radonc.2021.04.009.
[15] Bissonnette J-P, Yap ML, Clarke K, et al. Serial 4DCT/4DPET imaging to predict and monitor response for locally-advanced non-small cell lung cancer chemo-radiotherapy. Radiother Oncol 2018;126:347–54. https://doi.org/10.1016/j.radonc.2017.11.023.
[16] Huang W, Fan M, Liu B, et al. Value of metabolic tumor volume on repeated 18 F-FDG PET/CT for early prediction of survival in locally advanced non-small cell lung cancer treated with concurrent chemoradiotherapy. J Nucl Med 2014;55:1584–90. https://doi.org/10.2967/jnumed.114.142919.
[17] Gensheimer MF, Hong JC, Chang-Halpenny C, et al. Mid-radiotherapy PET/CT for prognostication and detection of early progression in patients with stage III non-small cell lung cancer. Radiother Oncol 2017;125:338–43. https://doi.org/10.1016/j.radonc.2017.08.007.
[18] Kanzaki H, Kataoka M, Nishikawa A, et al. Impact of early tumor reduction on outcome differs by histological subtype in stage III non-small-cell lung cancer treated with definitive radiotherapy. Int J Clin Oncol 2016;21:853–61. https://doi.org/10.1007/s10147-016-0982-0.
[19] Brink C, Bernchou U, Bertelsen A, et al. Locoregional control of non-small cell lung cancer in relation to automated early assessment of tumor regression on cone beam computed tomography. Int J Rad Oncol Biol Phys 2014;89:916–23. https://doi.org/10.1016/j.ijrobp.2014.03.038.
[20] Dooms C, Verbeken E, Stroobants S, et al. Prognostic stratification of stage IIIA-N2 non–small-cell lung cancer after induction chemotherapy: a model based on the combination of morphometric-pathologic response in mediastinal nodes and primary tumor response on serial 18-fluoro-2-deoxy-glucose positron emission tomography. JCO 2008;26:1128–34. https://doi.org/10.1200/JCO.2007.13.9550.
[21] William WN, Pataer A, Kalhor N, et al. Computed tomography RECIST assessment of histopathologic response and prediction of survival in patients with resectable non–small-cell lung cancer after neoadjuvant chemotherapy. J Thorac Oncol 2013;8:222–8. https://doi.org/10.1097/JTO.0b013e3182774108.
[22] McAleer MF, Moughan J, Byhardt RW, et al. Does Response to induction chemotherapy predict survival for locally advanced non–small-cell lung cancer? Secondary analysis of RTOG 8804/8808. Int J Rad Oncol Biol Phys 2010;76:802–8. https://doi.org/10.1016/j.ijrobp.2009.02.053.
[23] Møller DS, Holt MI, Alber M, et al. Adaptive radiotherapy for advanced lung cancer ensures target coverage and decreases lung dose. Radiother Oncol 2016;121:32–8. https://doi.org/10.1016/j.radonc.2016.08.019.
[24] Hoffmann L, Holt MI, Knap MM, et al. Anatomical landmarks accurately determine interfractional lymph node shifts during radiotherapy of lung cancer patients. Radiother Oncol 2015;116:64–9. https://doi.org/10.1016/j.radonc.2015.06.009.
[25] Horn KP, Thomas HMT, Vesselle HJ, et al. Reliability of quantitative 18F-FDG PET/CT imaging biomarkers for classifying early response to chemoradiotherapy in patients with locally advanced non-small cell lung cancer. Clin Nucl Med 2021;46:861–71. https://doi.org/10.1097/RLU.0000000000003774.
[26] Lodge MA, Chaudhry MA, Wahl RL. Noise considerations for PET quantification using maximum and peak standardized uptake value. J Nucl Med 2012;53:1041–7. https://doi.org/10.2967/jnumed.111.101733.
[27] Akamatsu G, Ikari Y, Nishida H, et al. Influence of statistical fluctuation on reproducibility and accuracy of SUV max and SUV peak: a phantom study. J Nucl Med Technol 2015;43:222–6. https://doi.org/10.2967/jnmt.115.161745.
[28] Lababede O, Meziane MA. The Eighth Edition of TNM Staging of Lung Cancer: Reference Chart and Diagrams. The Oncologist 2018;23:844–848. https://doi.org/10.1634/theoncologist.2017-0659.
[29] Nygård L, Vogelius IR, Fischer BM, et al. A competing risk model of first failure site after definitive chemoradiation therapy for locally advanced non-small cell lung cancer. J Thorac Oncol 2018;13:559–67. https://doi.org/10.1016/J.JTHO.2017.12.011.
[30] Katagiri Y, Jingu K, Yamamoto T, et al. Differences in patterns of recurrence of squamous cell carcinoma and adenocarcinoma after radiotherapy for stage III non-small cell lung cancer. Jpn J Radiol 2021;39:611–7. https://doi.org/10.1007/s11604-021-01091-y.
[31] Davey A, van Herk M, Faivre-Finn C, et al. Is tumour sphericity an important prognostic factor in patients with lung cancer? Radiother Oncol 2020;143:73–80. https://doi.org/10.1016/j.radonc.2019.08.003.
[32] Zwanenburg A, Leger S, Vallières M, Löck S. Image biomarker standardisation initiative. Radiology 2020;295:328–38. https://doi.org/10.1148/radiol.2020191145.
[33] Kim E, Wu H-G, Keam B, et al. Significance of 18F-FDG PET parameters according to histologic subtype in the treatment outcome of stage III non–small-cell lung cancer undergoing definitive concurrent chemoradiotherapy. Clin Lung Cancer 2019;20:e9–23. https://doi.org/10.1016/j.cllc.2018.08.018.
[34] Shepherd FA, Crowley J, Van Houtte P, et al. The International Association for the Study of Lung Cancer Lung Cancer Staging Project: Proposals Regarding the Clinical Staging of Small Cell Lung Cancer in the Forthcoming (Seventh) Edition of the Tumor, Node, Metastasis Classification for Lung Cancer. J Thorac Oncol 2007;2:1067–77. https://doi.org/10.1097/JTO.0b013e31815bdc0d.
[35] Schuurbiers OCJ, Meijer TWH, Kaanders JHAM, et al. Glucose metabolism in NSCLC is histology-specific and diverges the prognostic potential of 18FDG-PET for adenocarcinoma and squamous cell carcinoma. J Thorac Oncol 2014;9:1485–93. https://doi.org/10.1097/JTO.0000000000000286.
[36] Hörner-Rieber J, Bernhardt D, Blanck O, et al. Long-term follow-up and patterns of recurrence of patients with oligometastatic NSCLC treated with pulmonary SBRT. Clin Lung Cancer 2019;20:e667–77. https://doi.org/10.1016/j.cllc.2019.06.024.
[37] Mentink JF, Paats MS, Dumoulin DW, et al. Defining oligometastatic non-small cell lung cancer: concept versus biology, a literature review. Transl Lung Cancer Res 2021;10:3329–38. https://doi.org/10.21037/tlcr-21-265.
[38] Antonia SJ, Villegas A, Daniel D, et al. Overall survival with durvalumab after chemoradiotherapy in stage III NSCLC. N Engl J Med 2018;379:2342–50. https://doi.org/10.1056/nejmoa1809697.